

## On the c-Si/SiO<sub>2</sub> interface recombination parameters from photo-conductance decay measurements

Ruy S. Bonilla and Peter R. Wilshaw

Citation: *Journal of Applied Physics* **121**, 135301 (2017); doi: 10.1063/1.4979722

View online: <http://dx.doi.org/10.1063/1.4979722>

View Table of Contents: <http://aip.scitation.org/toc/jap/121/13>

Published by the *American Institute of Physics*

---

### Articles you may be interested in

[Hydrogenated amorphous silicon oxide \(a-SiO<sub>x</sub>:H\) single junction solar cell with 8.8% initial efficiency by reducing parasitic absorptions](#)

*Journal of Applied Physics* **121**, 133103 (2017); 10.1063/1.4979690

[Comparative study for highly Al and Mg doped ZnO thin films elaborated by sol gel method for photovoltaic application](#)

*Journal of Applied Physics* **121**, 135103 (2017); 10.1063/1.4979724

[Electrical properties of planar AlGaIn/GaN Schottky diodes: Role of 2DEG and analysis of non-idealities](#)

*Journal of Applied Physics* **121**, 135701 (2017); 10.1063/1.4979530

[Graphical analysis of current-voltage characteristics in memristive interfaces](#)

*Journal of Applied Physics* **121**, 134502 (2017); 10.1063/1.4979723

[Comparison of different bonding techniques for efficient strain transfer using piezoelectric actuators](#)

*Journal of Applied Physics* **121**, 135303 (2017); 10.1063/1.4979859

[Separation of the surface and bulk recombination in silicon by means of transient photoluminescence](#)

*Applied Physics Letters* **110**, 042105 (2017); 10.1063/1.4975059

---

Looking for a specific  
**instrument?**

Easy access to the latest equipment.  
Shop the *Physics Today* Buyer's Guide.



PHYSICS  
TODAY

lasers imaging  
VACUUM EQUIPMENT  
instrumentation  
software MATERIALS  
cryogenics + MORE...

# On the c-Si/SiO<sub>2</sub> interface recombination parameters from photo-conductance decay measurements

Ruy S. Bonilla and Peter R. Wilshaw

*Department of Materials, University of Oxford, Oxford OX1 3PH, United Kingdom*

(Received 7 November 2016; accepted 23 March 2017; published online 5 April 2017)

The recombination of electric charge carriers at semiconductor surfaces continues to be a limiting factor in achieving high performance optoelectronic devices, including solar cells, laser diodes, and photodetectors. The theoretical model and a solution algorithm for surface recombination have been previously reported. However, their successful application to experimental data for a wide range of both minority excess carrier concentrations and dielectric fixed charge densities has not previously been shown. Here, a parametrisation for the semiconductor-dielectric interface charge  $Q_{it}$  is used in a Shockley-Read-Hall extended formalism to describe recombination at the c-Si/SiO<sub>2</sub> interface, and estimate the physical parameters relating to the interface trap density  $D_{it}$ , and the electron and hole capture cross-sections  $\sigma_n$  and  $\sigma_p$ . This approach gives an excellent description of the experimental data without the need to invoke a surface damage region in the c-Si/SiO<sub>2</sub> system. Band-gap tail states have been observed to limit strongly the effectiveness of field effect passivation. This approach provides a methodology to determine interface recombination parameters in any semiconductor-insulator system using macro scale measuring techniques.

Published by AIP Publishing. [<http://dx.doi.org/10.1063/1.4979722>]

## I. INTRODUCTION

The reduction of carrier recombination is a key factor for improving the performance of optoelectronic devices, in particular, the energy conversion efficiency of semiconductor solar cells. When light is absorbed in a cell, charge carriers are generated and migrate to the semiconductor junction to be selectively collected. One of the main limiting factors in this process is the loss of minority charge carriers via recombination either in the bulk or at the surfaces of the solar cell. Bulk recombination occurs largely via impurities and structural defects. The semiconductor surface is also a defect-rich region where recombination of charge carriers is greatly enhanced. Since surfaces and interfaces cannot be avoided in a solar cell, reduction of surface recombination is of utmost importance. Moreover, with the increasing use of thinner substrates, surface recombination becomes a more critical obstacle, in comparison to bulk recombination, to achieve higher cell efficiencies.

In the last decade, major improvements have been achieved in processing techniques to reduce surface recombination using passivation layers. These comprise dielectric films that produce very low surface state densities, most notably, thermal silicon dioxide (SiO<sub>2</sub>),<sup>1</sup> remote plasma enhanced chemical vapour deposited (r-PECVD) silicon nitride (SiN),<sup>2-4</sup> and more recently, atomic layer deposited (ALD) and PECVD aluminium oxide (Al<sub>2</sub>O<sub>3</sub>).<sup>5-8</sup> The quality of surface passivation of those layers is generally characterized by the surface recombination velocity (SRV): It has been demonstrated that SiO<sub>2</sub>, SiN, and Al<sub>2</sub>O<sub>3</sub> produce SRVs as low as 2.4 cm/s,<sup>1</sup> 3.7 cm/s,<sup>9</sup> and 1.5 cm/s,<sup>10</sup> respectively, at an injection level of  $10^{15} \text{ cm}^{-3}$ , on float zone  $\sim 1.5 \Omega \text{ cm}$  n-type silicon.

The excellent surface passivation of these films is not only due to a chemical reduction in the density of interface states and/or their capture cross sections, but also to the

presence of fixed charge.<sup>7,11,12</sup> When charge is present in the dielectric film, an electric field is established at the interface, either attracting or repelling carriers from the surface. Repelling minority carriers from the surface limits their availability for recombination. This is known as field effect passivation (FEP). The passivation effect of most dielectric films is both chemical and field effect in origin; in practice, many dielectric films already have built-in electrostatic charge, so that FEP is already exploited.<sup>13</sup> The extent to which FEP might be utilised can be assessed via modelling of the SRV; yet the parameters used should be carefully defined so that theory accurately accounts for experimental measurements. This modelling is essential to establish optimum dielectric films and charge concentrations for surface passivation in current and new geometries of solar cells.

The physical nature and theoretical description of surface recombination were first considered by Fitzgerald and Grove.<sup>14</sup> An algorithm to solve the theory and analyse field effect passivation was then proposed by Girisch *et al.*<sup>15</sup> using an extended version of the Shockley-Read-Hall (SRH) theory of recombination.<sup>16,17</sup> This was later extended by Aberle *et al.*<sup>18,19</sup> to include the steady-state generation of minority carriers by illumination. In these works, SRV was modelled as a function of both dielectric charge density and minority carrier injection; however, the experimental data used were limited to a single value of dielectric charge. For this reason, the modelled dependence of SRV for a range of dielectric charges could not be verified. Girisch's model also predicted values of SRV well below 1 cm/s when moderate ( $\sim 10^{11} \text{ q/cm}^2$ ) charge was present in the dielectric. Such SRVs have not been observed experimentally in succeeding work on the Si/SiO<sub>2</sub> interface.<sup>18,20,21</sup> Additionally, an increase in SRV has been experimentally observed at low minority carrier injection levels, which is not accounted for in the aforementioned

model. Several reports have addressed this discrepancy by proposing an enhanced recombination region near the surface, the so-called surface damage region, yet this hypothesis remains unsupported by direct experimental evidence.<sup>22–24</sup> Multiple modelling studies have followed those of Girisch and Aberle. Dauwe *et al.*<sup>25</sup> and Weber *et al.*,<sup>26</sup> for example, modelled SRV or (equivalently) dark saturation current  $J_{0e}$  for a single value of minority carrier injection and varied the dielectric charge concentration. On the other hand, Kho *et al.*<sup>21</sup> reported lifetime data, from which SRV can be extracted, for a range of carrier injections and positive dielectric charge densities, yet their proposed model parameters did not fit the experimental data. Most recently, Haug *et al.*<sup>27,28</sup> proposed an original method to characterise SRV using photoluminescence (PL) imaging and a direct metal contact to the dielectric to control field effect passivation. In this method, the SRV was measured using a fixed photon flux, thus corresponding to different injections levels. They successfully used Girisch's model to find the interface recombination parameters that fitted the observed SRV data, yet the accuracy of the model for a wide range of carrier injections could not be verified. To the author's knowledge, a report of SRV modelling that includes a wide range of both independent variables, minority excess carrier density and fixed dielectric charge, has not been produced. In general, when the reported data have been fitted to only one of the two independent variables, the same modelling parameters do not provide a correct dependency on the remaining variable.

In this paper, we report a detailed investigation of the different parameters involved in modelling surface recombination velocity using the extended SRH formalism as set by Girisch. We apply the model to study FEP of a silicon dioxide – silicon interface, and we provide a reliable prediction of surface recombination velocity over a wide range of both independent variables: dielectric fixed charge and excess minority carrier concentration. This modelling describes interface recombination without the need to introduce a term for the surface damage region which, in the case of a thermally grown oxide/silicon interface, is thought to be physically unreasonable. It also separates the contribution of interface trap states and a field effect towards total surface recombination. Further, the methodology allows estimation of electron and hole surface recombination velocities, interface trap density, and the capture cross sections without requiring complicated experimental procedures such as deep level transient spectroscopy. In the following, we give a detailed description of the extended SRH formalism with particular emphasis on interface charge. Subsequently, we use the model to interpret the results obtained from a corona-lifetime experiment on oxide passivated Float Zone (FZ) silicon wafers. By fitting the experimental data over a wide range of both independent variables, we produce a set of parameters that accurately describe surface recombination at the oxide-silicon interface.

## II. THEORY

### A. Shockley-Read-Hall surface recombination

In 1952, Shockley and Read, and later Hall, reported the first comprehensive study of injection dependent

recombination of carriers via defects.<sup>16,17,29</sup> They proposed a recombination rate as a result of detailed balance of emission and capture rates of both electrons and holes via a single defect located at an energy  $E_t$ . When the same recombination model is applied to the semiconductor surface, two important modifications need to be applied. First, the semiconductor surface is a large crystal discontinuity and as such it produces a continuum of defect states in the band-gap that has to be considered. Second, the physical concept of carrier lifetime becomes ambiguous since it is expressed for carriers traveling to the surface rather than in the bulk, hence the need to define the surface recombination velocity. Surface recombination ( $U_s$ ) is described by extending the Shockley-Read-Hall formalism to an arbitrary trap level density function<sup>15</sup>

$$U_s = \int_{E_v}^{E_c} \frac{(n_s p_s - n_i^2)}{\frac{[n_s + n_1(E)]}{v_{th} D_{it}(E) \sigma_p} + \frac{[p_s + p_1(E)]}{v_{th} D_{it}(E) \sigma_n}} dE, \quad (1)$$

where  $n_i$  is the Si intrinsic carrier density,  $D_{it}$  is the energy dependent density of interface traps,  $v_{th}$  is the thermal velocity of both types of carriers,  $\sigma_n, \sigma_p$  are the capture cross sections for electrons/holes, and  $n_s$  and  $p_s$  are the carrier concentrations at the surface defined as

$$n_s = n_b e^{\frac{\phi_{scr}}{kT/q}} \quad p_s = p_b e^{\frac{-\phi_{scr}}{kT/q}}, \quad (2)$$

where Boltzmann statistics have been used with  $n_b$  and  $p_b$  being the bulk carrier concentrations, and  $n_1/p_1$  the carrier concentrations for when the Fermi level falls to  $E$ , defined as

$$n_1 = n_i e^{\frac{E-E_i}{kT}} \quad p_1 = n_i e^{\frac{E_i-E}{kT}}. \quad (3)$$

It is noted that Fermi-Dirac statistics, using Seiwatz and Green treatment,<sup>30</sup> did not produce a significant difference in the modelling formalism yet required substantial computing power and for that reason Boltzmann statistics were preferred. The surface recombination velocity, disregarding recombination in the band-bent region, is then obtained as

$$S_{eff} \equiv \frac{U_s}{\Delta n} = \frac{1}{\Delta n} \int_{E_v}^{E_c} \frac{(n_s p_s - n_i^2)}{\frac{[n_s + n_1(E)]}{S_p} + \frac{[p_s + p_1(E)]}{S_n}} dE, \quad (4)$$

where  $\Delta n$  is the excess minority carrier concentration,  $S_p(E) = v_{th} D_{it}(E) \sigma_p(E)$  is the energy dependent recombination velocity for holes, and  $S_n(E) = v_{th} D_{it}(E) \sigma_n(E)$  is the energy dependent recombination velocity for electrons. Physically,  $S_p$  and  $S_n$  represent the maximum rate at which holes and electrons are captured independently.  $S_{eff}$ , on the other hand, comprises the total recombination occurring at the surface as a result of capture of both types of carriers.

An important distinction needs to be made between recombination at the physical location of the interface ( $S_0$ ) and the effective surface recombination ( $S_{eff}$ ). In thermal equilibrium, the energy bands are flat throughout the semiconductor (for uniform doping and defect density). However, in practical semiconductors, a space charge region (SCR) is

normally present at the surface, thus creating a small region where the conduction and valence bands bend, due to charge near or trapped at the interface. In general, the effective SRV is defined as that seen by the bulk at the edge of the space charge region  $d_{scr}$  such that  $S_{eff} = U_s / \Delta n(z = d_{scr})$ . Additionally, recombination happening in the SCR can originate from near-surface defects and changes in the carrier concentration, and should be included in the total surface recombination velocity. For this purpose, recombination that takes place within the band-bent region is considered a component of surface recombination, and recombination in a flat-band region is considered bulk recombination. A more general definition is the total SRV

$$S_{total} \equiv \frac{U_{z < d_{scr}}}{\Delta n_{d_{scr}}} = S_{eff} + S_{scr}, \quad (5)$$

where the  $z$  axis is perpendicular to the semiconductor surface and increases towards the bulk, with  $d_{scr}$  being the edge of the space charge region.  $S_{scr}$  represents the recombination taking place in the SCR, while  $S_{eff}$  only includes recombination due to surface states.  $S_{eff}$  is also a more useful metric as it is possible to infer it directly from measurements of effective lifetime in well characterised samples. This will become evident in Section III.

### B. The effect of surface band bending

In practical semiconductors, surface band bending is nearly always present, even in the absence of dielectric charge. Intrinsic band bending arises from charged states at the semiconductor surface, which are in turn balanced by near-surface semiconductor charge. Such surface trap states may be donor type (become positively charged when they donate an electron) or acceptor type (become negatively charged when they accept an electron). The total charge in surface defect states is therefore given by the sum of ionized donor and acceptor states

$$Q_{it} = q \int_{E_v}^{E_c} D_{it,d}(E) f_d(E) dE - \int_{E_v}^{E_c} D_{it,a}(E) (1 - f_d(E)) dE, \quad (6)$$

where the subscripts  $d$  and  $a$  in  $D_{it}$  indicate donor and acceptor-like states, respectively.  $f_d$  is the trap occupation probability for holes in donor states given by the SRH recombination model as<sup>18</sup>

$$f_d = \frac{n_1 + S_r p_1}{(n_s + n_1) + S_r(p_s + p_1)}, \quad (7)$$

where  $S_r = S_p / S_n$  is the ratio between the hole and electron surface capture rate, here referred to as the cross section asymmetry since  $S_p / S_n = \sigma_p / \sigma_n$ .

Regardless of the origin of semiconductor surface charge, the end result is a net change in the concentration of carriers at the surface. These depend both on the minority carrier injection level ( $\Delta n$ ) and the band bending, defined as the semiconductor potential at the surface  $\phi_{scr} = \phi(z = 0)$ . Figure 1 illustrates the band diagram and charge

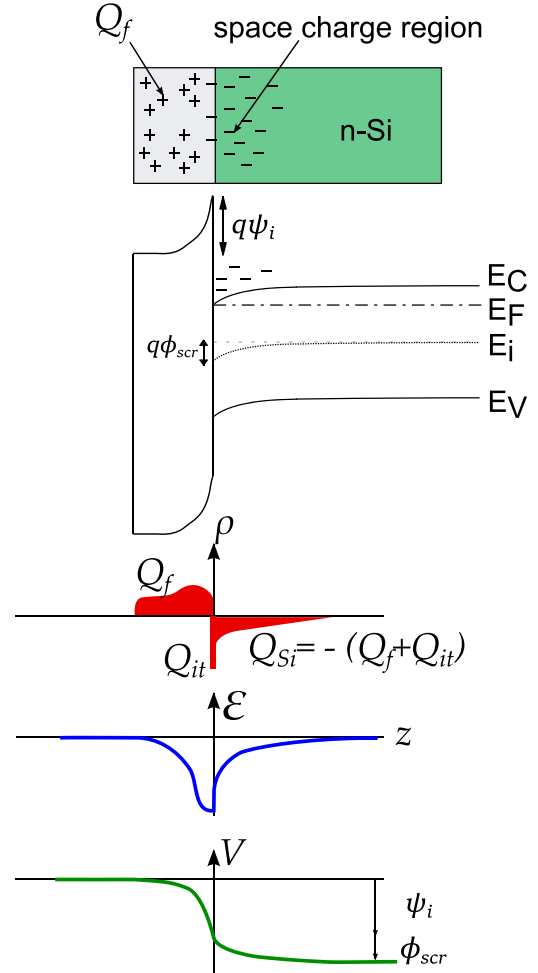


FIG. 1. Schematic representation of the band bending problem at the surface of silicon due to charge present near and at the interface with a dielectric film.

concentration of a semiconductor/dielectric interface when charge in the semiconductor balances fixed charge in the dielectric layer  $Q_f$ .  $Q_f$  is compensated by charge in the semiconductor both at filled interface defects, and in the near-surface space charge region (SCR). Computing  $\phi(z)$  requires the simultaneous use of Poisson's equation and the continuity equations describing carrier dynamics. Such a solution can only be found using finite element simulation packages such as Sentaurus<sup>31</sup> and PC1D.<sup>32</sup> However, a numerical solution can be obtained by assuming that the quasi-Fermi energy levels are constant throughout the SCR. This assumption has been previously proven reasonable.<sup>33</sup> Such a calculation is achieved by following an iterative procedure outlined by Girisch *et al.*<sup>15</sup> and extended by Aberle *et al.*<sup>18</sup> to include the steady-state generation of minority carriers by illumination.

### C. Recombination in the space charge region

Recombination that takes place within a bent-band region (by distinction to that occurring at the interface states) also contributes to surface recombination as previously stated in Equation (5). It is found by integrating the volumetric SCR recombination rate  $U_{sc}$  over its depth



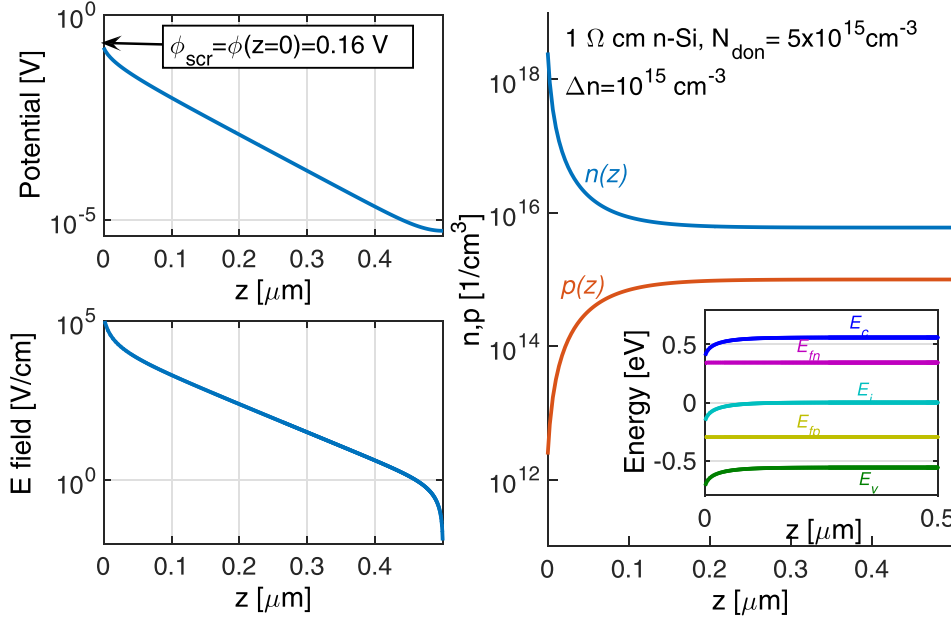


FIG. 2. Computed electric potential, field and carrier concentration for 1  $\Omega$  cm n-Si with a surface band bending of 0.15 V, and photo-injected with  $10^{15} \text{ cm}^{-3}$  minority charge carriers,  $T = 300 \text{ K}$ . The inset depicts the energy levels with respect to the intrinsic energy.

$$S_{scr} = \int_0^{d_{scr}} U_{scr}(z) dz, \quad (8)$$

where the  $z$  axis is perpendicular to the semiconductor surface and increases towards the bulk, with  $d_{sc}$  being the edge of the space charge region. The integration in (8) requires the knowledge of carrier density as a function of distance from the surface  $n(z)$ ,  $p(z)$ , and the surface band bending  $\phi(z)$ . Such a calculation can only be done numerically. Example solutions can be found in detail in Mönch's book.<sup>34</sup> Here, a numerical solution to Poisson's equation was found using a finite difference method that implements a Lobatto IIIa formula in Matlab.<sup>35</sup> For 1  $\Omega$  cm n-Si, for example, a space region charge of  $-10^{12} \text{ q/cm}^2$  is produced when the SCR potential (band bending) is  $\sim 0.16 \text{ V}$ , with an excess minority carrier concentration of  $10^{15} \text{ cm}^{-3}$  (calculated using Equation (B2a) in Ref. 15). Figure 2 illustrates the  $n(z)$ ,  $p(z)$  calculated from a numerical solution to Poisson's equation for this scenario including uniform photo-generation of  $10^{15} \text{ cm}^{-3}$  carriers. The electric field and potential have also been included as they are the result of solving Poisson's equation.

Recombination in the SCR can be Auger, radiative and SRH type

$$S_{scr} = \frac{1}{\Delta n} \int_0^{d_{sc}} (U_{Aug}(z) + U_{rad}(z) + U_{SRH}(z)) dz$$

$$S_{scr} = \frac{1}{\Delta n} \int_0^{d_{sc}} C_n(n^2 p - n_0^2 p_0) + C_p(np^2 - n_0 p_0^2) + B(np - n_i^2) + \frac{np - n_i^2}{\tau_{n0}(p + p_1) + \tau_{p0}(n + n_1)} dz, \quad (9)$$

where  $n = n(z)$  is the semiconductor electron concentration as a function of depth, and  $p = p(z)$  is the hole concentration as a function of depth. All other parameters are defined equivalently to Richter's parametrisation in Ref. 10. The edge of the space charge region was here defined as the depth at which the minority carrier concentration is within

1% its value in the bulk region. Figure 3 illustrates the contribution of recombination in the SCR towards the overall surface recombination velocity for both polarities of charge—i.e., upward and downward band-bending, such that a space charge region of approximately  $\pm 10^{12}$  is produced when  $\Delta n = 10^{15} \text{ cm}^{-3}$ . The Auger and radiative components, and the SRH component of SCR recombination have been plotted independently. When positive charge is present in the semiconductor surface, an inversion region is formed in n-type silicon surface and thus, at a characteristic depth from the surface, the concentration of both types of carrier equalizes, and the defect-mediated recombination is enhanced. This explains the higher  $S_{scr,SRH}$  for positive  $Q_{Si}$  in Figure 3. Regardless of the charge polarity, recombination in the SCR contributes less than 0.1 cm/s of the total surface recombination at medium and low injection levels. Significant SCR recombination ( $\geq 0.2 \text{ cm/s}$ ) only occurs when the SRH defects in the SCR act as efficient recombination centres—i.e., low electron and hole lifetime, for example, when  $\tau_{p0} = \tau_{n0} < 1 \text{ ms}$ . Overall, the SCR contributes negligibly to the

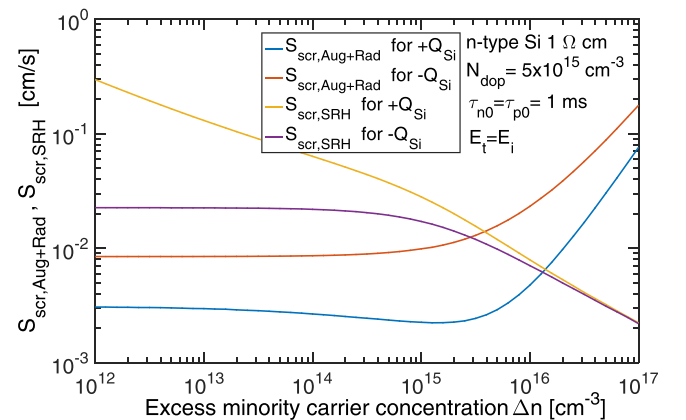


FIG. 3. Computed space charge region recombination for 1  $\Omega$  cm n-Si with a surface potential of  $-0.22(+0.18) \text{ V}$ , such that a surface charge concentration of  $+(−)10^{12} \text{ q/cm}^2$  is present,  $T = 300 \text{ K}$ . Auger recombination is calculated using Richter's parameterization.<sup>10</sup>

surface recombination velocities measured in practice, as will become evident in Section III, and thus it has been disregarded in the rest of the calculations.

#### D. Recombination in a near-surface region

Early reports on the theory of surface recombination in Si/SiO<sub>2</sub> predicted values of SRV well below 1 cm/s with moderate concentrations of dielectric charge. Experimentally, these were not observed, and even more an increase in SRV was seen at low minority carrier injection levels, contrary to what theory predicted. Glunz *et al.*<sup>20</sup> were first to address these discrepancies by suggesting three extensions to the SRH formalism: in-homogeneities in charge distribution, carrier recombination in the space charge region (SCR) due to tunnelling, and carrier recombination at highly active surface bad spots. Charge in-homogeneities can be of two kinds. First, micro-scale intrinsic fixed charge in the oxide gives rise to surface potential fluctuations in the order of  $\sim kT/q$ .<sup>20,36</sup> Second, large-scale non-uniformity of dielectric surface charge, for example, corona deposited, gives rise to larger fluctuations. The latter can be verified using Kelvin Probe and capacitance-voltage (C-V) maps of dielectric charge,<sup>37</sup> and can be minimized as shown in Ref. 38. SCR recombination was argued to arise from carrier tunnelling towards surfaces states and carriers recombining in an enhanced recombination region near the surface,<sup>20,25</sup> yet experimental evidence of neither was reported, in particular, for the Si/SiO<sub>2</sub> system. Moreover, for many years thermally grown silicon dioxide has been the basis for MOSFET technology and no evidence of such near surface recombination has been found. Using these additions, Glunz *et al.* modelled the SRV dependence on both dielectric charge and minority carrier concentration, but fitting of theory to experimental data was only carried out using a single independent variable; either one minority carrier injection level or one dielectric charge concentration.

Recently, a region of enhanced recombination near the surface has been suggested to explain the increased SRV at low injection levels.<sup>22</sup> This has been defined as a surface-damaged region (SDR). Section IIC showed that recombination in the space charge region is only significant when near-surface defects have sufficiently low lifetime, thus the need to introduce near surface damage into the modelling formalism—e.g., Ref. 22–24. Despite the seemingly good model of SRV, the SDR hypothesis lacks a reasonable physical basis as there is no experimental evidence that such a defect region exists, at least for the case of a thermal Si/SiO<sub>2</sub> interface. For the general case of chemical and physical vapour deposited dielectrics,<sup>39,40</sup> the surface damage region is a possibility due to ion and radiation bombardment. The development of the model in Sections IIE–IIF will show that, for a thermally grown SiO<sub>2</sub> on Si, SRV can be described without introducing a term for near-surface recombination and is thus able to fully account for the surface carrier dynamics. Given the arguments covered in Sections IIC and IID in what follows  $S_{total} = S_{eff}$ .

#### E. The effect of electron and hole recombination in effective SRV

Previously reported calculations of SRV have used direct measurements of the density of interface traps ( $D_{it}$ ) and the hole and electron capture cross sections ( $\sigma_{p,n}$ ). These have been obtained using the DLTS technique and the Conductance-Voltage method<sup>41</sup> and have been input directly into the SRH formalism. The accuracy of DLTS characterisation of  $D_{it}$  and  $\sigma_{n,p}$  depends strongly on the signal-to-noise ratio of the measured transients, the level of accuracy of the temperature measurement, the extent of the temperature range, and method of evaluation used.<sup>42–45</sup> As with the present method, DLTS relies on simulations,<sup>46</sup> yet it only provides values of  $D_{it}$  and  $\sigma_{n,p}$  for half of the band-gap for each type of doping,<sup>47</sup> thus needing two different samples to study the entire band-gap. Although these studies provided a remarkable insight into the Si/SiO<sub>2</sub> interface, in particular, for the development of MOSFET technology, the  $D_{it}$  and  $\sigma_{p,n}$  extracted from them have not produced an accurate characterisation of the macro-scale SRV, especially when carrier injection and dielectric charge are considered together in a broad domain. Haug<sup>27,28</sup> and Chen<sup>48</sup> have recently obtained accurate models by lumping together the  $D_{it} \times \sigma_{n,p}$  product into the  $S_{p,n}(E)$  parameter, and extracting empirical values for the latter such that theory fits experimental data. Here, a similar approach is taken where  $S_{n,p}$  values are used to find a good empirical fit of experimental SRV.  $S_{p,n}(E)$  lumps the two fundamental interface properties together in the same way that carrier lifetime is used in the single defect SRH model, yet in the surface case  $S_{p,n}$  is an energy dependent parameter. The effect of this parameter on the effective SRV will now be studied using previously reported data as the basis to parametrise  $S_{p,n}$  with respect to energy.

$D_{it}$  and  $\sigma_{p,n}$  are energy dependent quantities commonly, yet not necessarily correctly, parametrised as Gaussian functions.<sup>20</sup> Measurements of  $D_{it}$  using Terman's,<sup>49</sup> Berglund's,<sup>50</sup> Castagne and Vapaille's,<sup>51</sup> or Nicollian and Goetzberger's<sup>41</sup> methods showed that an inverse Gaussian function best described the dependence of  $D_{it}$  with energy. Similarly,  $\sigma_{p,n}$  measured via DLTS<sup>18,52</sup> has been previously described by a Gaussian function. The product between an inverse Gaussian function and a Gaussian function is Gaussian too. Previous models have shown that the energy dependence of  $\sigma_{p,n}$  is larger than that of  $D_{it}$ . This means that in their product, the dependence of  $\sigma_{p,n}$  would prevail over that of  $D_{it}$ . The resulting function is therefore Gaussian. With the aim of understanding how the energy dependence affects the total recombination velocity, the independent capture of electron and holes will be parametrised as

$$S_{p,n} = S_{0p,n} e^{-a_{n,p}(E-E_{0p,n})^2}, \quad (10)$$

where  $S_{0n/p}$  is the mid-value of the function, which characterises the maximum surface recombination rate for each carrier type at an energy  $E_{0p,n}$  (the centre of the function).  $a$  is the curvature of the function, which represents how strongly  $S_{n,p}$  depends on the energy where the trap states are located. It is noted that the exponential dependency followed here

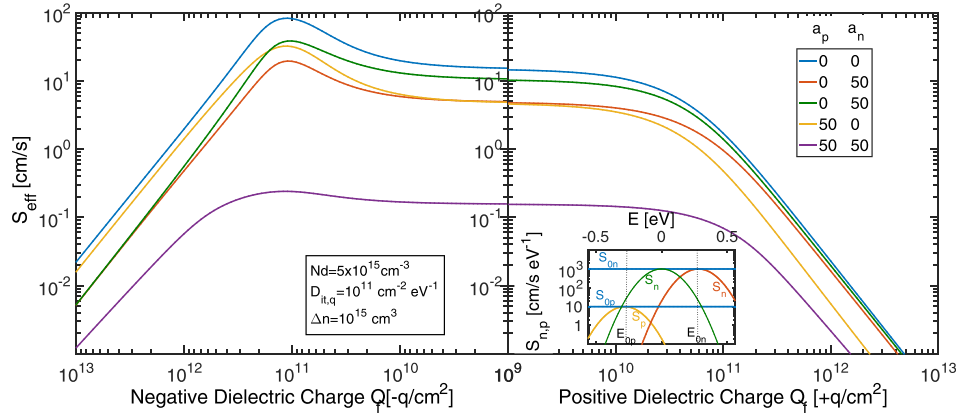


FIG. 4. Surface recombination velocity for n-type silicon as a function of positive and negative dielectric fixed charge concentration in  $\text{q}/\text{cm}^2$ , for an excess minority carrier concentration of  $10^{15} \text{ cm}^{-3}$ , and a variation in the surface recombination of holes and electrons given by the curvatures  $a_n$  and  $a_p$ . Four combinations of  $a_n$ ,  $a_p$  have been chosen as illustrated by the legend in the figure. Inset: Hole (yellow) and electron (red) surface recombination functions used to calculate surface recombination velocity. Blue horizontal lines represent the value the functions take when the dependence on energy is eliminated ( $a_0 = 0$ ).

was chosen because it matches the commonly reported data; it does not suggest its correctness for all semiconductor/dielectric interfaces. In fact, studies that used Nicollian and Goetzberger's conductance method in the Si/SiO<sub>2</sub> system show that  $\sigma_{p,n}$  is largely energy independent in the mid-gap region, while it decreases rapidly at band edges.<sup>53–55</sup> These parametrisations are used as a first approximation to understand how  $S_{eff}$  is affected by different energy dependencies in  $S_{n,p}$ .

Figure 4 illustrates the influence of Equation (10) on Equation (4) for typical reported values of the parameters. Here,  $S_{eff}$  increases whenever the mid-value ( $S_{0n/p}$ ) increases for either holes or electrons. However, if the dependence of  $S_{eff}$  on fixed dielectric charge  $Q_f$  is considered, it is clear that surface recombination is governed by  $S_{0n}$  when negative charge is present in the dielectric, or by  $S_{0p}$  when positive charge is present in the dielectric. This can be inferred from the carrier concentrations at the surface. When positive charge exists in the dielectric, holes in the semiconductor are repelled from the surface, while electrons are attracted. Recombination is dependent on the concentration of both types of electrical carriers, and it is limited by the less available carrier, in this case the holes. Consequently, for a given positive and negative dielectric charge concentration, the minimum value of  $S_{eff}$  is given by  $S_{0p}$  and  $S_{0n}$ , respectively. The maximum value of  $S_{eff}$ , on the other hand, depends on both  $S_{0p}$  and  $S_{0n}$ , and occurs when the concentration of electrons and holes at the surface is balanced so that  $S_n n_s = S_p p_s$ . This occurs at a moderate ( $\sim 10^{11} \text{ q}/\text{cm}^2$ ) negative dielectric charge concentration for n-type Si, or positive charge for p-type Si.

The dependence of  $S_{n,p}$  on energy is given by the function curvature  $a_{p,n}$ , which can only take positive values. When the curvature of either function increases,  $S_{p,n}$  decreases around its maximum,  $S_{0p,n}$  at  $E_0$ , and a smaller tail of states is observed towards the centre, inset in Figure 4. Smaller values of  $S_{p,n}$  mean slower capture of carriers, so that the larger the curvature, the smaller the effect on the total  $S_{eff}$ . Increasing the curvature of  $S_p$  reduces surface

recombination for positive dielectric charge and increasing the curvature of  $S_n$  reduces it for negative dielectric charge. If both hole and electron SRV functions have a high curvature parameter, then the overall recombination is reduced as illustrated by the purple trace in Figure 4.

The centre or axis of the SRV Gaussian functions determines the energy in the band-gap where recombination is most likely to happen. For the case in Figure 4, the functions are centred at one quarter of the band-gap energy above the valence band for holes, and below the conduction band for electrons. This follows capacitance-voltage and deep level transient spectroscopy data reported in the literature.<sup>20</sup> Similar to the standard SRH theory, deep level impurities are stronger recombination centres than shallow level impurities. Moving the function axis ( $E_{0p,n}$ ) is equivalent to shifting the energy level of the maximum recombination rate. Hence, when the maximum is moved towards the centre of the band-gap, i.e., deeper, the probability of recombination is increased and the surface recombination velocity also increases. This effect, however, only applies to low dielectric charge concentrations ( $|Q_f| < 10^{11} \text{ q}/\text{cm}^2$ ) where mid-gap recombination is dominant. For large dielectric charge concentrations, on the other hand,  $S_{eff}$  is largely insensitive to the energy dependence of  $S_n, S_p$ . In such a regime, deeper states only marginally increase the total recombination. An example of this is given by the green trace in Figure 4, where the capture of electrons has been increased by shifting toward deeper states. Here, an increase in  $S_{eff}$  is seen for low dielectric charge concentrations ( $|Q_f| < 10^{11} \text{ q}/\text{cm}^2$ ), while approximately the same  $S_{eff}$  is observed for  $|Q_f| > 10^{11} \text{ q}/\text{cm}^2$  regardless of where the  $S_n$  function is centred in the bandgap. Furthermore, for high positive dielectric charge, where recombination is limited by the available holes,  $S_{eff}$  is approximately the same as when  $S_n$  is energy-independent. This indicates that despite proposing an energy dependent parametrisation of electron and hole capture, their energy-dependence does not influence overall SRV significantly. The energy dependence of  $S_{n,p}$  will be considered when applying this model to real data for the sake of completeness,

yet, in fact, Section III will reveal that even if this parametrisation the  $S_{n,p}$  value is used, empirically extracted values are largely energy independent.

### F. The effect of interface charge concentration

In Section II E,  $D_{it}$  and  $\sigma_{p,n}$  were lumped into the surface recombination velocities for holes and electrons ( $S_{p,n}$ ). In order to calculate the concentration of charge at the interface,  $Q_{it}$  in Equation (6), a separate parameter is introduced here to represent the concentration of surface interface states that get charged when band bending occurs, termed  $D_{it,q}$ . The calculation of  $Q_{it}$  is the subject of this section.

Semiconductor interface charge strongly influences the value of SRV. When dielectric charge is compensated in the semiconductor, some of this compensating charge can be found occupying interface states rather than modifying the near-surface carrier concentration. The higher the concentration of states at the surface, the fewer the carriers needed in the semiconductor to compensate the dielectric charge, and therefore, a smaller change in surface carrier concentration occurs and recombination is not as effectively reduced. Although  $D_{it,q}$  has been typically described by an inverse Gaussian function, additional extensions have been proposed by adding exponential tail functions to model the high density of states near the band edges.<sup>20,56</sup> Despite the high density of such near band tail states, they contribute negligibly to the recombination activity at the surface. This is a consequence of the extended SRH process as described in Section II E. In this work, a three term exponential function is proposed to model  $D_{it,q}$ . The first term represents the mid-gap density of interface states  $D_{itq0}$ , the second density of states near the conduction band-edge, and the third the density of states near the valence band-edge

$$D_{it,q}(E) = D_{itq0} + D_{itC}e^{m_C E + E_{0C}} + D_{itV}e^{m_V E + E_{0V}}, \quad (11)$$

where  $E_{0C,V}$  and  $m_{C,V}$  define the rate with which the tail of states approach  $D_{itC}$  at the conduction band edge, and  $D_{itV}$  at the edge valence band edge. At the middle of the gap, the density of charged states is  $D_{itq0}$ . As suggested by Sze, it is useful to define a neutral energy level  $E_0$  that separates acceptor-like and donor-like traps in the band-gap.<sup>57</sup> The

total charge in surface defect states is therefore given by a modified form of Equation (6)

$$Q_{it} = q \int_{E_V}^{E_0} D_{it,d}(E) f_d(E) dE - \int_{E_0}^{E_C} D_{it,a}(E) (1 - f_d(E)) dE, \quad (12)$$

where  $E_V$  and  $E_C$  represent the band edge energies. The value  $E_0$  takes has been previously suggested to be near the mid-gap.<sup>36,56</sup> Simulations conducted in Section III showed that a value of neutral energy  $E_0$  in the range  $-E_g/4 < E_0 < +E_g/4$  had a negligible effect on SRV, as can also be inferred from Girisch's treatment,<sup>15</sup> and thus, a value  $E_0 = E_g/2$  is assumed throughout this work. In general, changes in the dielectric fixed charge can produce changes in both donor and acceptor states at the interface. However, as will become clear in Section III, the purpose of such  $E_0$  is mainly to separate the nature of the band tail states between donor-type near the valence band, and acceptor-type near the conduction band. Distinguishing the nature of the interface states is a complex task.<sup>36</sup> However, previous reports have shown that it is a reasonable assumption to consider the valence band tail of donor-type, and the conduction band tail of acceptor-type states.<sup>54,57-60</sup>

The effect of  $D_{itq0}$  on  $S_{eff}$  is first explored in Figure 5 (blue and orange curves), by assuming  $D_{itC} = D_{itV} = 0$ . Values of  $S_{p/n}$  and  $D_{itq0}$  commonly reported in the literature were used and  $S_p, S_n$  were kept constant so that variations in  $D_{itq}$  only affected the interface charge concentration and not the carrier dynamics. An increase in the mid-gap trap density  $D_{itq0}$  is seen to increase  $S_{eff}$  for small values of dielectric charge  $|Q_f| < 10^{11} \text{ q/cm}^2$ . This is a direct consequence of having more charge stored in surface traps, rather than compensated in the space charge region. As more states become available at the interface, less charge is compensated as space charge and the field effect is lost, allowing for more recombination at the surface. This is an important effect, as it indicates that if better chemical passivation is provided (smaller  $D_{it,q}$ ), the effectiveness of dielectric charge to produce FEP is increased and hence, less charge is necessary in the dielectric. Note that this effect is in addition to that normally associated with chemical passivation, namely, that a reduction in surface states directly reduces the number of sites available for recombination. Conversely, if not enough chemical passivation is provided, then effective passivation

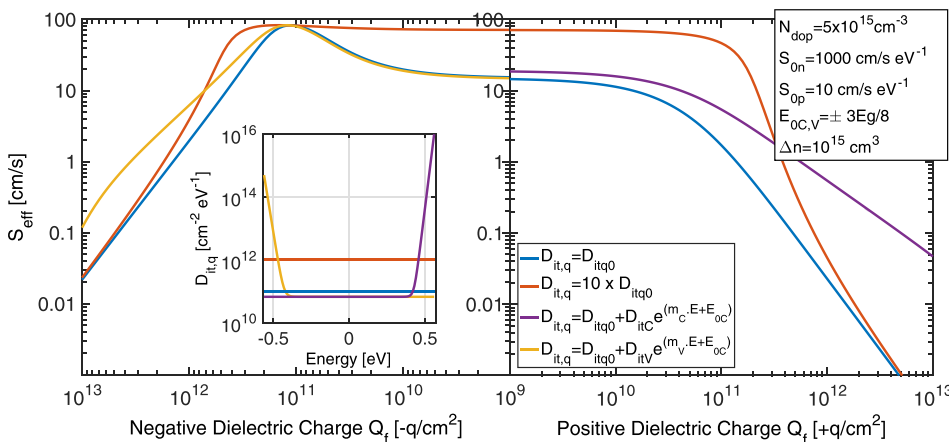


FIG. 5. Effective surface recombination velocity for n-type silicon as a function of positive and negative dielectric fixed charge concentration, for an excess minority carrier concentration of  $10^{15} \text{ cm}^{-3}$ , and a variation in the charge stored at surface states  $Q_{it}$ , given by the dependence on  $D_{it}$ .



can only be achieved using substantial concentrations of dielectric charge.

The increase in  $D_{it,q}$  near the band-edges is represented by the second and third terms in Equation (11). When  $D_{it,q}$  increases near the conduction band, i.e., higher  $D_{itC}$ ,  $S_{eff}$  is seen to decrease its dependence on charge for positive dielectric charge (purple curve in Figure 5), but no change is observed for negative dielectric charge (blue curve in Figure 5). This change of dependence (slope) is due to the increased compensating charge present at interface states rather than in the near surface SCR. In the absence of such defect state charge concentration, the number of electrons in the conduction band would be higher and  $S_{eff}$  would be further reduced. Similarly, when  $D_{it,q}$  increases near the valence band ( $D_{itV}$ ),  $S_{eff}$  dependence with negative dielectric charge decreases, since a bigger portion of the compensating positive charge is now present at interface states rather than in the SCR (yellow trace in Figure 5). The dependence of  $S_{eff}$  on interface compensated charge has been found to be a very important parameter involved in modelling  $S_{eff}$ , as will become clear in the Section III when analysing experimental data.

### G. Discussion

This section has set out the theoretical model required to describe carrier recombination at the silicon/dielectric interface. An extended Shockley-Read-Hall formalism was used, and carrier dynamics parameters ( $\sigma, D_{it}$ ) were lumped together into a parameter that relates directly to the velocity with which electrons and holes are independently captured at the surface. The use of electron and hole capture velocities will allow an easier search for empirical parameters to fit experimental data. The influence of recombination in the space charge region and in a near-surface damage region was calculated. It was concluded that Auger and radiative recombination in the space charge region are negligible. In the case of surface damage, it was noted that near-surface recombination was significant if deep recombination centres with electron and hole lifetimes below 1 ms were produced by the damage in the near-surface region. For a thermal  $\text{SiO}_2/\text{Si}$  interface, no physical basis could be suggested to explain such damage recombination centres, and thus, their contribution was neglected in the effective SRV calculations performed here.

The charge concentration at the interface  $Q_{it}$  was parametrised independent of the recombination velocity of electrons and holes. This parametrisation has proven to be advantageous in understanding recombination at the oxide/silicon interface, particularly when considering the influence of interfacial charge. It was shown that  $Q_{it}$  greatly influences the dependence of  $S_{eff}$  with  $Q_f$ , especially for high concentrations of charge where the band tail states play a significant role. The dependence on minority carrier injection was not addressed above. However, when SRV is studied as a function of both the injection level and the dielectric charge concentration, these parametrisations can help infer the interface recombination characteristics ( $D_{it,q}, S_n, S_p$ ) between silicon and a dielectric film. This will be demonstrated in Section III using thermally grown silicon dioxide as a case study.

### III. APPLICATION TO OXIDE PASSIVATED n-type c-Si

This section presents a case of study of the modelling parametrisation described, and serves to demonstrate the effectiveness of externally applied charge, namely, extrinsic field effect passivation (FEP).<sup>61</sup> Previous research has mainly focused on the effect of the surface charge on the effective lifetime of silicon for one excess minority carrier concentration or one surface charge density.<sup>62–64</sup> Here, the dependence of surface recombination velocity on both independent variables is explored. An investigation of excess minority carrier concentration from  $10^{14}$  to  $10^{16} \text{ cm}^{-3}$  and dielectric charge concentration from  $-2 \times 10^{12}$  to  $7 \times 10^{12} \text{ q/cm}^2$  is performed. By exploring both variables simultaneously, it is possible to infer values for the fundamental interface properties so as to produce the best fit to the experimental data obtained. The methodology to study the effect of charge on FEP of silicon is first described. Experimental lifetime data are then converted to SRV and the modelling formalism is applied to find the parameters that describe this  $\text{Si}/\text{SiO}_2$  interface.

#### A. Experimental methods

Experimental data on the relation between surface recombination and dielectric charge were obtained. Sample preparation, processing, and measurements were carried out in an immediate sequence so that a possible influence of time variations could be discounted:  $1 \Omega \text{ cm}$ ,  $4''$  n-type FZ-Si wafers were dry oxidized at Fraunhofer ISE to provide the base passivation film, resulting in an oxide thickness of  $100 \pm 1 \text{ nm}$  as measured via reflectance spectrometry. These were then deposited with a fixed concentration of charge via corona discharge, immediately followed by a photoconductance decay lifetime measurement and a measurement of charge concentration via Kelvin Probe (KP). This three step measurement methodology (corona charge – lifetime – KP) was repeated until the change in lifetime with increasing charge was minimal.

In order to deposit charge, a custom-built point-to-plane corona discharge apparatus was used. Using this apparatus, potentials between  $-30$  to  $+30 \text{ kV}$  were applied to a steel needle for negative or positive charging at a distance of  $20 \text{ cm}$ . The measurements of the charge deposited on the dielectric were performed using a modified version of the Scanning Kelvin Probe 3.1 by KP Technology Ltd.,<sup>65</sup> and Baikie's method.<sup>66</sup> Mapping was performed using a non-feedbacked XY stage actuated by stepper motors. Kelvin probe measurements had a  $\sim 0.2 \text{ mm}$  lateral resolution, and they were taken in the centre of the specimens, consequently they only represented a small region of surface charge. Mapping was used to find the optimal potential and distance in the corona discharge set up. The overall charge concentration of the surface was kept within 5% uniformity as shown in Ref. 38. Figure 6 illustrates a schematic picture of the methodology used and a surface potential map that demonstrates highly uniform corona discharge deposition – uniformity better than 3.5%, Figure 6 inset.

To determine the charge concentration from KP measurements, the charge induced potential as a function of

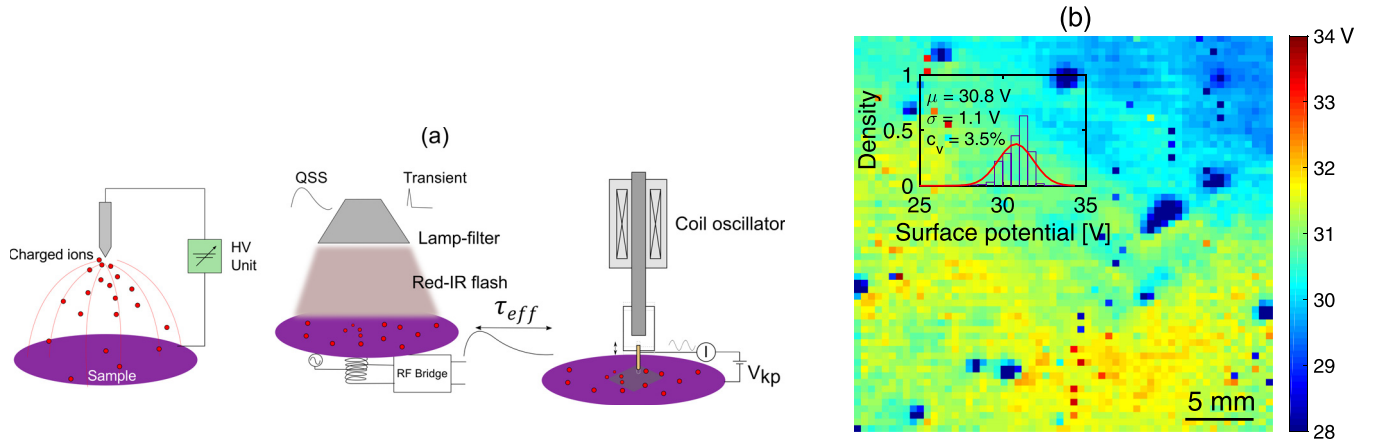


FIG. 6. (a) Schematic of corona charge – lifetime – KP methodology, (b) Kelvin Probe surface potential map of a specimen charged with positive corona discharge. Inset: probability density function of surface potential.

charge density and the insulator-semiconductor characteristics is calculated as<sup>67</sup>

$$V_{KP} = \frac{\Phi_{ms}}{q} + \frac{1}{K_i \epsilon_0} \int_0^{t_i} x \rho(x) dx + \phi_{scr}, \quad (13)$$

where  $\Phi_{ms}$  is the work function difference between the metal tip and the semiconductor,  $t_i$  is the thickness of the dielectric coating,  $\rho(x)$  is the volumetric charge concentration in the dielectric, and  $\phi_{scr}$  is the surface potential drop in the semiconductor. If the KP measurements are performed right after charge deposition, it can be assumed that most of the charge resides at the surface as a charge per unit area ( $\sigma$ ). Equation (13) then becomes

$$V_{KP} = \frac{\Phi_{ms}}{q} + \frac{t_i \sigma}{\epsilon_i} + \phi_{scr}. \quad (14)$$

Charge density at the surface can thus be calculated from

$$\sigma = \left( V_{KP} - \frac{\Phi_{ms}}{q} - \phi_{scr} \right) \epsilon_i / t_i, \quad (15)$$

when the dielectric films are sufficiently thick, the surface potential measured is of the order several volts, and thus, the internal semiconductor surface potential can be disregarded in Equation (15). This allows an estimation of the surface charge concentration  $\sigma$ . Despite this, for the modelling performed here the surface potential in Equation (14) was used as the independent variable instead of the dielectric fixed charge concentration. This avoided inaccuracies arising from the value of  $\phi_{scr}$ .  $\Phi_{ms}$  was obtained by measuring the contact potential between the KP tip and a bare piece of silicon wafer, i.e., without the grown oxide.

One additional measurement is necessary since, as indicated from Equation (13), Kelvin Probe measurements cannot distinguish the charge in the bulk of the film from charge on the surface. Dielectric films normally exhibit an intrinsic charge concentration, which generally resides very close to the oxide-semiconductor interface and therefore is hardly detected by KP measurements. A charge offset has to be measured by different means in order to produce an accurate

value. In our work, high frequency capacitance-voltage measurements were taken on specially fabricated metal-oxide-semiconductor (MOS) dots from the same wafers. Eight measurements were taken across the wafer and an average flat-band voltage shift of  $\sim -182$  mV was observed, equivalent to an initial charge concentration of  $\sim +4.2 \times 10^{10}$  q/cm<sup>2</sup>. This value was then added to the corona deposited charge to calculate the total dielectric charge.

Surface recombination was assessed by measuring effective lifetime using a Sinton WCT-120 photo-conductance instrument,<sup>68,69</sup> with a precision better than 8% according to Ref. 70. The effective minority carrier lifetime for a silicon wafer as a whole can be expressed as the reciprocal sum of the bulk and the surface components

$$\frac{1}{\tau_{eff}} = \frac{1}{\tau_B} + \frac{1}{\tau_s}. \quad (16)$$

Increasing both these lifetimes is the key in improving solar cell efficiency. The bulk component, including Auger and radiative recombination, is assumed to be described by Richter's parameterisation, Equation (18) in Ref. 10, using  $B_{rel}$  from Ref. 71 and  $B_{low}$  from Ref. 72.

The surface lifetime component has an elaborate dependence on SRV. The amount of recombination at the surface depends on the spatial variation of the injected carriers. Carriers generated far from the surface may only recombine when they diffuse to the surface. Similarly, carriers generated at the surface may recombine instantaneously or diffuse to the bulk. To account for this dependence, Luke and Cheng<sup>73</sup> developed a formalism and found a solution that indicates that the effective SRV is a function of an infinite sum of decaying exponential terms of effective lifetime. The first mode is dominant and it is written as

$$S_{eff} = \sqrt{D_p \left( \frac{1}{\tau_{eff}} - \frac{1}{\tau_b} \right)} \tan \left( \frac{W}{2} \sqrt{\frac{1}{D_p} \left( \frac{1}{\tau_{eff}} - \frac{1}{\tau_b} \right)} \right). \quad (17)$$

For sufficiently low SRV,  $\tan(x) \approx x$ , and this expression can be simplified to the typically used equation  $S = W/2 (\tau_{eff}^{-1} - \tau_b^{-1})^{-1}$ . However, when surface carrier concentrations are modified via the field effect, the SRV can increase

considerably such that Equation (17) must be used. The diffusion coefficient of holes in n-type silicon was calculated using the online PV Lighthouse tool.<sup>74</sup>

Recent reports have shown that high purity float zone silicon can develop point defects thus lowering its bulk lifetime.<sup>75,76</sup> When calculating SRV, a lower bulk lifetime would lead to lower values of SRV. To account for this, the lower limit of the error bars in  $S_{eff}$  was calculated using a bulk lifetime affected by an extrinsic Shockley-Read-Hall defect. Here, a single mid-gap defect with  $\tau_{p0} = 10 \times \tau_{n0}$  was used.

Finally, a 30 mm  $\times$  5 mm specimen was cut off the wafer previously used for lifetime measurements. This was used for a resistivity measurement using the 4-probe technique. Four 0.5 mm wide by 5 mm long, InGa stripes were painted on this specimen. Resistance was then measured using a Keithley SMU yielding a resistivity of 0.92  $\Omega$  cm, thus a phosphorous doping concentration of  $5.4 \times 10^{15} \text{ cm}^{-3}$ , according to the calculator in Ref. 75.

### B. The effect of corona charge on effective lifetime

The measured effective lifetime as a function of total dielectric charge is illustrated in Figure 7. For this sample, negative polarity charge was first deposited and an increase in effective lifetime was recorded, Figure 7(a). As predicted from theory, an initial decrease in effective lifetime (higher SRV) is observed when small concentrations of negative charge are present on the dielectric. The starting charge concentration is represented by the dark blue down-pointing triangle line with  $V_{kp} = -0.02$  V, equivalent to  $Q_f = -4 \times 10^{10} \text{ q/cm}^2$ . Negative charge is then deposited to take the surface potential to  $-0.14$  V, orange trace. Maximum recombination (minimum lifetime) is observed when  $V_{kp} = -1.32$  V, yellow trace. Further deposition of negative charge then reduces surface recombination (increases lifetime) as shown by the subsequent light blue trace,  $V_{kp} = -1.97$  V, and then onwards. Afterwards, the sample was rinsed with IPA to remove charge<sup>77</sup> and positive polarity charge was deposited in similar steps, Figure 7(b). Upon positive charge deposition, lifetime directly increased as a result of improved surface passivation via FEP as expected from the theory. The dielectric charge was taken from  $V_{kp} = -1.18$  V ( $-3 \times 10^{11} \text{ q/cm}^2$ ) to  $V_{kp} = +34.17$  V ( $7.3 \times 10^{12} \text{ q/cm}^2$ ), increasing effective lifetime over 3.3 ms at an injection of  $10^{15} \text{ cm}^{-3}$ . Figure 7(b) also includes the Auger and radiative intrinsic lifetime limit. An extrinsic mid-gap SRH bulk defect with  $\tau_{p0} = 10 \times \tau_{n0} = 8 \text{ ms}$  was included to evaluate the effect of possible bulk deterioration during oxide growth. Curves where the effective lifetime is below 200  $\mu$  s were measured using quasi steady state PCD instead of transient PCD as suggested by Sinton.<sup>68</sup>

### C. Modelling surface recombination for Si/SiO<sub>2</sub>

Field effect passivation provided by dielectric charge has been demonstrated to reduce surface recombination and thus increase the effective lifetime of oxide passivated silicon. In order to apply the modelling formalism in Section II, experimental lifetimes must be translated to values for SRV at the Si/SiO<sub>2</sub> interface, Equation (17). Figure 8 illustrates

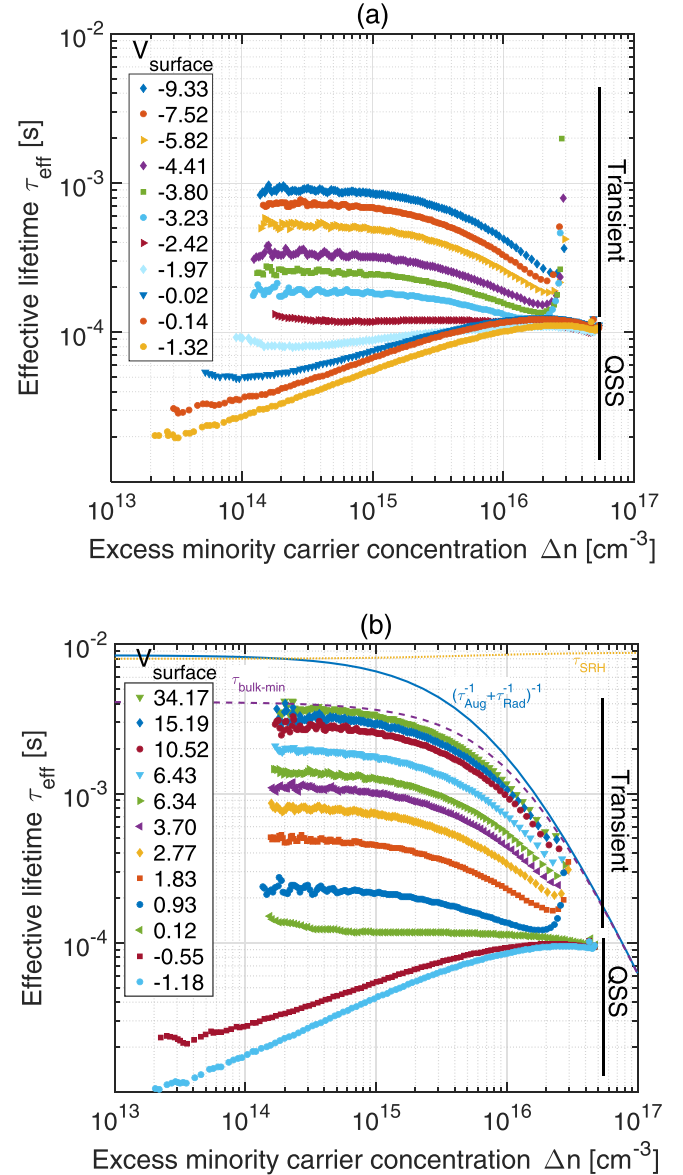


FIG. 7. Lifetime measurements of n-type (100) FZ Silicon (0.92  $\Omega$ cm) passivated with a 100 nm-thick thermal oxide, for (a) negative and (b) positive corona deposited surface charge.

SRV as a function of positive and negative dielectric charge concentration  $Q_f$  for three different minority carrier injection levels  $\Delta n$ . Markers in Figure 8 indicate the measured values of  $S_{eff}$ , while the solid lines represent the theoretically calculated  $S_{eff}$ . These values of  $\Delta n$  were chosen as the most representative in the domain of interest,  $10^{14}$ – $10^{16} \text{ cm}^{-3}$ . Error bars were calculated using the minimum SRV possible when a SRH bulk defect is present, and were only drawn when bigger than the curve markers. Using the theory set out in Section II, values for  $D_{it,q}$ ,  $S_n$ , and  $S_p$  were found so that the model best fitted the experiments. The search for parameters started from known previously reported values,<sup>18,20,56</sup> and those calculated from results of C-V measurements.<sup>38,56</sup> The optimal fitting parameters were found by minimising the least-squared weighted errors between modelled and the measured data. The value of each parameter was kept within a range where they were physically meaningful, while still



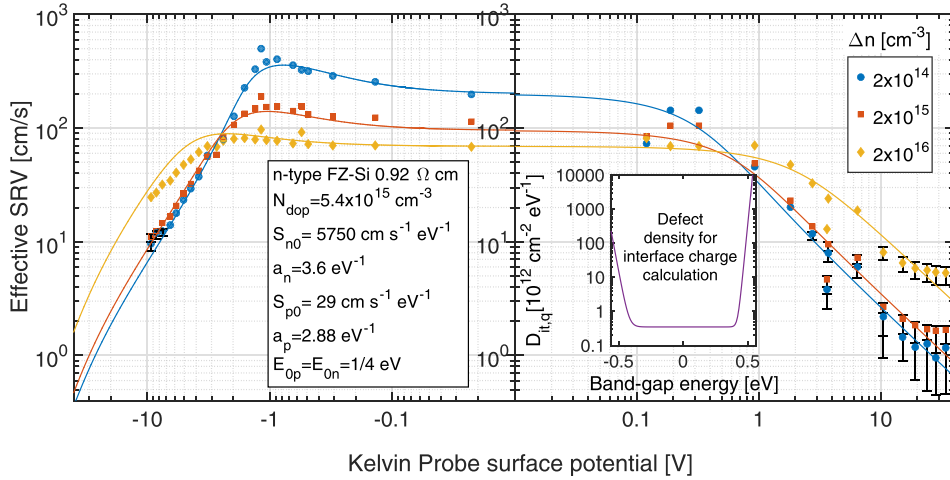


FIG. 8. Surface recombination velocity measurements and simulations as a function of negative (left) and positive (right) corona deposited surface charge [ $q/\text{cm}^2$ ], for three excess minority carrier concentrations.

providing a good agreement between theory and experiments. Figure 8, however, only illustrates three minority injection levels. Injection dependent plots of SRV for different values of dielectric charge are illustrated in Figure 9 for the same set of measurements as in Figure 7. The surface potential used in the simulated curves, however, differed from the ones measured via KP, previously quoted in Figure 7. The difference between the two is illustrated in the inset in Figure 9. Showing that significant error only occurs for very high charge concentrations and thus surface potentials. For high charge concentrations,  $V_{KP} > 10\text{ V}$ , the accuracy of charge measurements using KP is reduced due to the high values of KP surface potential measured. When the KP potential measured is outside the bias range of the instrument ( $-10\text{ V}$ ,  $10\text{ V}$ ), extrapolation is required as described by the Baikie method,<sup>66</sup> and the accuracy is reduced. However, the difference between modelled and measured  $Q_f$  taken here is acceptable considering that the uniformity of the measured dielectric charge concentration was  $\sim 3.5\%$ , as reported previously for this set of specimens. Additionally, at high surface potentials, surface recombination is minimal and thus, the influence of SRH bulk defect is more evident, as illustrated by the large error bars for  $S_{eff} < 10\text{ cm/s}$ .

#### D. Discussion

This section has presented experimental evidence of the reduction in surface recombination achieved via FEP in agreement with past work.<sup>18,20,21,28</sup> For this, an experimental methodology has been set up to extrinsically modify and measure the concentration of charge on a  $\text{SiO}_2$  film. A characterisation of the uniformity of charge was conducted and the methods used produced surface charge uniformity to better than 5%. When deposition of surface charge is sufficiently controlled, the large-scale surface potential fluctuations can be disregarded, especially given the scale ( $\sim\text{cm}$ ) of lifetime and surface potential measurements. The first extension proposed by Glunz *et al.* in Ref. 20 has therefore not been used here. The presence of small-scale fluctuations was not characterised here since its influence in the observed SRV values is limited to surface potentials in the  $\pm 0.5\text{ V}$  range, for a  $\text{Si}/\text{SiO}_2$  system with  $< 5 \times 10^{10}\text{ q/cm}^2$  intrinsic charge.<sup>36</sup> Effective lifetime was recorded as a function of

minority carrier concentration and total dielectric charge concentration, as presented in Figure 7. These data show the effectiveness of FEP in reducing surface recombination. An increase in effective lifetime of over 30-fold was demonstrated between as grown oxide and corona passivated specimens, with SRV values approaching  $1\text{ cm/s}$  for mid and low injection levels. This shows the outstanding potential of FEP further building on similar previous reports.<sup>21,26,78</sup> The influence of such low recombination on solar cell efficiency is difficult to assess due to other factors in the cell fabrication process. Nonetheless, modelled solar cells have been reported to obtain up to 2% absolute increase in efficiency due to reduced surface recombination.<sup>79,80</sup> The possibility of such an increase in efficiency confirms that controlled and extrinsic FEP is a potential method for providing surface passivation to industrial scale solar cells, particularly when the techniques, as used here, are fast and inexpensive. The outstanding issue for such controlled field effect passivation is the stability of the charge. Additional work by the same authors has provided evidence of stable and controlled FEP.<sup>61</sup>

Figure 7 also shows the difference in passivation provided by positive versus negative charges. This asymmetry is a characteristic feature of the interfacial physical properties and had been first pointed out by Girisch<sup>15</sup> when setting the surface SRH model. It can be quantified by computing the ratio  $S_{eff}(+Q_f)/S_{eff}(-Q_f)$  as previously suggested by Haug *et al.*<sup>28</sup> This value relates to the ratio of surface recombination of holes to that of electrons  $S_r = S_{p0}/S_{n0}$ , and hence, it provided an indication of the values  $S_{n,p}$  should take in the theoretical model. For example, for the  $\text{Si}/\text{SiO}_2$  system studied here recombination for positive charge was more effective than for negative,  $S_{eff}(+Q_f)/S_{eff}(-Q_f) \leq 0.2$  leading to  $S_{p0}/S_{n0} \ll 0.2$ . This condition helps the search for parameters that best describe the  $S_{eff} = f(Q_f, \Delta p)$  relation, which includes  $S_n$ ,  $S_p$ ,  $D_{it0}$ ,  $D_{itV}$ , and  $D_{itC}$ .

The reported set of corona-lifetime measurements have been all performed on a single c-Si/dielectric system, and included a range of both dielectric charge concentration, and minority carrier injections. This extended investigation of both variables allowed a more accurate search of parameters. This has not been normally considered except for the work



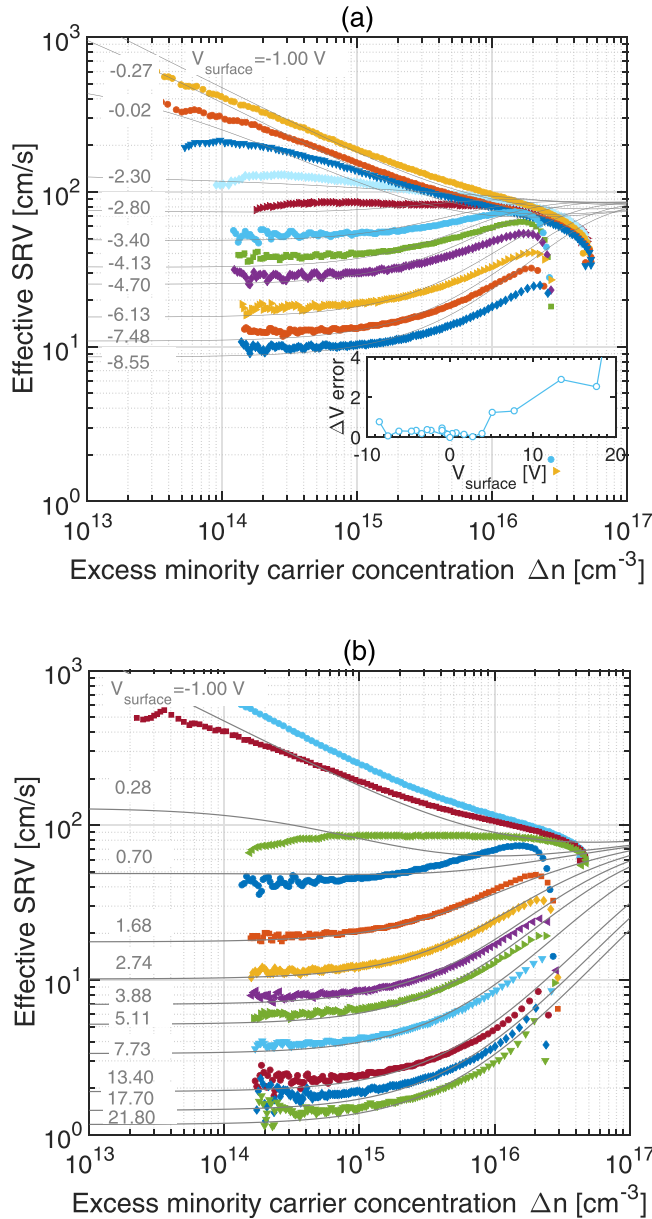


FIG. 9. Surface recombination velocity measurements and simulation for n-type FZ Silicon passivated with a 100 nm thermal oxide with (a) negative and (b) positive surface dielectric charge. These data are the equivalent SRV from data shown in Figure 7. The inset depicts the difference between the surface potential measured and used in the modelled SRV.

of Kho *et al.*<sup>21</sup> who reported the effect of positive charge on effective lifetime of oxide passivated n-type FZ silicon. Their measurements differed from those shown here in several aspects: first, in their work the minority concentration at which the lifetime is at a maximum is  $10^{15} \text{ cm}^{-3}$ , with a prominent peak. Kho *et al.* attributed such a peak to surface recombination, in particular, when the peak reduced in prominence with increasing dielectric charge. Second, in their work a decreased lifetime for low injection levels is observed after corona charging, which was not observed on this work. Here, effective lifetime increases almost uniformly for all carrier injections, when  $V_{\text{surface}} > 0.5 \text{ V}$ . Additionally, the intrinsic passivation of the Si/SiO<sub>2</sub> interface for the specimens used here was of poorer quality, as evidenced from the lower effective lifetimes prior to any corona charge.

However, when deposited with charge, the effective lifetime measured in this work exceeded by over 3-fold that of Kho *et al.*

The theoretical formalism outlined in Section II was used to find the best modelling parameters that described the Si/SiO<sub>2</sub> interface. The search for parameters was conducted by plotting the experimental  $S_{\text{eff}}$  as a function of  $Q_f$ , for three indicative minority carrier injection levels, and then performing a parameter sweep using the frame of reference set by the parametrisation proposed in Sections II E–II F. Figure 8 illustrates this plot including the set of parameters that best described the experimental data. The values of  $S_n$  and  $S_p$  reflect the asymmetry observed for negative dielectric charge, the value of  $D_{itq0}$  reflects the independence of SRV on dielectric charge for low concentrations ( $|Q_f| < 10^{11} \text{ q/cm}^2$ ), and  $D_{itC}, D_{itV}$  reflect the degree of dependence that SRV exhibits with charge for large concentrations of both positive and negative dielectric charge. In fact, the information drawn in Figure 5 has shown that for the high dielectric charge conditions, the rate of reduction of SRV with field effect is more strongly related to  $D_{itC}, D_{itV}$  than to  $S_{p,n}$ . This would indicate that the concentration of interface charge stored in the band tails limits strongly the effectiveness of FEP.

The parameters found here are comparable to those previously inferred using other techniques as reported in Ref. 18, 56, and 78. They show a moderate chemical passivation component and a low FEP component in the as-grown oxide. An estimation of the commonly reported  $D_{it}$  and  $\sigma_{n,p}$  parameters is possible by assuming  $D_{it} = D_{it,q}$  and calculating  $\sigma_{n,p} = S_{n,p}(E)/v_{th}D_{it,q}(E)$ . These are depicted in Figure 10. Three key aspects are highlighted here: first, the asymmetry between the capture of electrons and holes is close to that previously reported  $S_r \sim 0.01$ . Second, although literature reports  $D_{it}$  and  $\sigma_{n,p}$  highly dependent on energy in the band gap, the values obtained here are largely independent with the exception of band edges or tails; furthermore, their product  $S_{n,p} \sim D_{it} \times \sigma_{n,p}$  is largely independent of energy. This can be a consequence of the lack of sensitivity that SRV has on the energy dependence of  $S_{p,n}$  as mentioned in Section II E. Since in SRH statistics band-edge states cause negligible recombination, the capture cross sections for such states tend to be neglected, while those for states near the mid gap

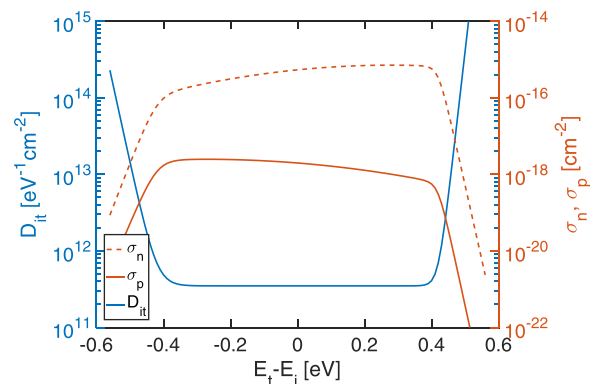


FIG. 10. Interface recombination parameters deduced from the model parameters used in Section III C.

are in the order of  $10^{-16} \text{ cm}^2$ . Third, the donor and acceptor band tail states are the limiting mechanism for the effectiveness of field effect passivation at large dielectric charge concentrations.

The accuracy of the theoretical model was further tested by producing injection dependent curves of SRV and fitting them to the experimentally measured ones. Figure 9, in contrast to Figure 7, depicts the surface recombination velocity reduction for all carrier injections studied here. These data demonstrate that  $S_{\text{eff}} < 1.5 \text{ cm/s}$  @  $\Delta n = 10^{15} \text{ cm}^{-3}$  can be achieved using controlled FEP. To the authors' knowledge, such a recombination velocity is among the lowest passivation schemes reported in the literature.<sup>1,13,81</sup> This is equivalent to dark saturation current densities of  $J_{0e} < 5 \text{ fA/cm}^2$  when calculated using approximation (3) in Ref. 82,  $J_{0e} = SRV * qn_i^2 / (N_{\text{dop}} + \Delta p)$ . Disagreement between experimental and modelled curves, for the low charge regime,  $V_{KP} < \pm 1 \text{ V}$  ( $Q_f < \pm 10^{11} \text{ q/cm}^2$ ), may arise from the lack of uniformity of the intrinsic charge in the oxide which was not assessed in the present work. The solid grey lines in Figure 9 show the best theoretical fits of  $S_{\text{eff}}$ , where the dielectric charge concentration was used as the fitting parameter while  $S_n$ ,  $S_p$ ,  $D_{it0}$ ,  $D_{itV}$ , and  $D_{itC}$  remained constant. The values of charge used for these fits corresponded well to those measured using KP (inset in Figure 9), thus indicating that the SRH model and parametrisations used are a good representation of surface recombination at the Si/SiO<sub>2</sub> interface.

$S_{\text{eff}} = f(Q_f, \Delta n)$  can also be plotted for the entire domain of both independent variables studied here. Figure 11 illustrates such a plot, where dielectric charge is swept from  $-10^{13}$  to  $+10^{13} \text{ q/cm}^2$  and carrier injection from  $10^{13}$ – $10^{17} \text{ cm}^{-3}$ . At low carrier injection levels,  $S_{\text{eff}}$  is strongly dependent on the concentration of charge present on the dielectric. As the minority carrier injection increases, the dependence reduces and dielectric charge does not reduce recombination as effectively. Maximum recombination occurs at negative charge for all levels of injection, when both electrons and holes are captured with the same probability ( $S_{nn_s} = S_{pp_s}$ ). A moderate depletion of electrons from the n-type silicon surface is therefore required to achieve such maximum recombination. The asymmetry of  $S_{\text{eff}}$  with dielectric charge polarity is also clear in Figure 11, with positive charge reducing recombination more effectively than negative charge. However, this is not necessarily true for all dielectric semiconductor interfaces and if, for a particular material system,  $S_p > S_n$  then the best passivation would be achieved with negative charge.

The present work has demonstrated that a complete analysis of the  $S_{\text{eff}} = f(Q_f, \Delta n)$  relation using the extended SRH formalism is sufficient to model recombination at certain semiconductor surfaces, given a correct parametrisation of the interface phenomena. It is believed that the analysis will be generally applicable to many other passivating dielectrics in addition to the Si/SiO<sub>2</sub> combination experimentally investigated here. However, it should be noted that the present work does not rule out the need to account for the presence of a SDR if dielectrics have been deposited by plasma techniques in such a way that a damaged region of

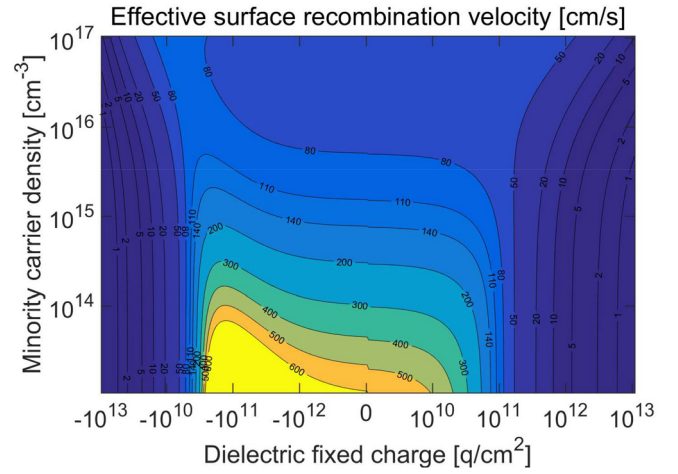


FIG. 11. Simulation of effective surface recombination velocity for 1  $\Omega \text{ cm}$  FZ n-type silicon passivated with SiO<sub>2</sub>, as a function of dielectric fixed charge and excess minority carrier concentration. Simulation parameters are given in Figure 9. Notice the x-axis on this figure is not a logarithmic axis.

semiconductor is produced at the interface with the dielectric.

#### IV. CONCLUSIONS

We have reviewed the theoretical formulation of recombination at the surface of a semiconductor, which has provided a powerful methodology to infer average interface parameters used when modelling crystalline silicon solar cells. The experimental data presented here demonstrated a large lifetime improvement in n-type FZ-Si by using corona discharge field effect passivation, leading to  $SRV \sim 1\text{--}2 \text{ cm/s}$ ,  $J_{0e} < 5 \text{ fA/cm}^2$ . Optimal surface passivation is key to high efficiency crystalline silicon solar cells, especially as the importance of surface physical processes increases when cell designs become thinner.

Calculations of SRV showed that the Shockley-Read-Hall formalism can be successfully used to describe the recombination at the FZ-Si/SiO<sub>2</sub> interface. For this, the interface parameters were parametrised and the dependence on both carrier injection and dielectric charge was considered when calculating the effective surface recombination velocity. The experimental and measurement procedures proved to be a good tool to characterize the properties of the thermal SiO<sub>2</sub>/c-Si interface, providing values for the product between the interface trap density  $D_{it}$  and capture cross sections  $\sigma_n$ ,  $\sigma_p$  in the mid-gap region. If all interface states are assumed to be charged, the approximation  $D_{it} = D_{it,q}$  can be used to infer values for the capture cross sections  $\sigma_{n,p}$  without the need for DLTS or multi-frequency Capacitance/Conductance-Voltage measurements.

For the FZ-Si/SiO<sub>2</sub> interface, we conclude that the electron capture rate, and hence their capture cross section, is higher than for holes, to a similar extent to what has been previously suggested in the literature.<sup>15</sup> The product  $S_{n,p} \sim D_{it} \times \sigma_{n,p}$  was found largely independent of energy. And finally, charging of the donor and acceptor band tail states largely limited the extent to which field effect passivation can reduce recombination at the interface. This methodology

can be extended to other interfaces provided that the charge is stable for at least the time of the experiment, and in this way, the properties and the extent of field effect passivation can, in general, be deduced for dielectric-semiconductor interfaces.

## ACKNOWLEDGMENTS

R. S. Bonilla is the recipient of an EPSRC (UK) Postdoctoral Research Fellowship, EP/M022196/1. P. R. Wilshaw acknowledges the support from EPSRC Grant No. EP/M024911/1. Both authors are thankful to Martin Hermle and Christian Reichel at Fraunhofer ISE for provision of oxidised silicon. Data published in this article can be downloaded from <http://ora.ox.ac.uk>.

- <sup>1</sup>M. J. Kerr and A. Cuevas, *Semicond. Sci. Technol.* **17**, 35–38 (2002).
- <sup>2</sup>A. G. Aberle, *Sol. Energy Mater. Sol. Cells* **65**, 239–248 (2001).
- <sup>3</sup>W. Soppe, H. Rieffe, and A. Weeber, *Prog. Photovoltaics* **13**, 551–569 (2005).
- <sup>4</sup>J. Schmidt and A. G. Aberle, *J. Appl. Phys.* **85**, 3626–3633 (1999).
- <sup>5</sup>F. Werner, B. Veith, V. Tiba, P. Poodt, F. Roozeboom, R. Brendel, and J. Schmidt, *Appl. Phys. Lett.* **97**, 162103 (2010).
- <sup>6</sup>J. Schmidt, F. Werner, B. Veith, D. Zielke, S. Steingrube, P. P. Altermatt, S. Gatz, T. Dullweber, and R. Brendel, *Energy Procedia* **15**, 30–39 (2012).
- <sup>7</sup>B. Hoex, J. J. H. Gielis, M. C. M. van de Sanden, and W. M. M. Kessels, *J. Appl. Phys.* **104**, 113703 (2008).
- <sup>8</sup>B. Hoex, S. B. S. Heil, E. Langereis, M. C. M. van de Sanden, and W. M. M. Kessels, *Appl. Phys. Lett.* **89**, 42112 (2006).
- <sup>9</sup>S. Duttagupta, F. Lin, M. Wilson, M. B. Boreland, B. Hoex, and A. G. Aberle, *Prog. Photovoltaics Res. Appl.* **22**, 641–647 (2014).
- <sup>10</sup>A. Richter, S. W. Glunz, F. Werner, J. Schmidt, and A. Cuevas, *Phys. Rev. B* **86**, 165202 (2012).
- <sup>11</sup>A. G. Aberle, *Prog. Photovoltaics* **8**, 473–487 (2000).
- <sup>12</sup>J. Schmidt, F. M. Schuurmans, W. C. Sinke, S. W. Glunz, and A. G. Aberle, *Appl. Phys. Lett.* **71**, 252 (1997).
- <sup>13</sup>Y. Larionova, V. Mertens, N.-P. Harder, and R. Brendel, *Appl. Phys. Lett.* **96**, 32105 (2010).
- <sup>14</sup>D. J. Fitzgerald and A. S. Grove, *Surf. Sci.* **9**, 347–369 (1968).
- <sup>15</sup>R. B. M. Girisch, R. P. Mertens, R. F. Dekeersmaecker, and R. F. De Keersmaecker, *IEEE Trans. Electron Devices* **35**, 203–222 (1988).
- <sup>16</sup>W. Shockley and W. T. Read, *Phys. Rev.* **87**, 835–842 (1952).
- <sup>17</sup>R. N. Hall, *Phys. Rev.* **87**, 387 (1952).
- <sup>18</sup>A. G. Aberle, S. Glunz, and W. Warta, *J. Appl. Phys.* **71**, 4422–4431 (1992).
- <sup>19</sup>A. Aberle, S. Glunz, and W. Warta, *Sol. Energy Mater. Sol. Cells* **29**, 175–182 (1993).
- <sup>20</sup>S. W. Glunz, D. Biro, S. Rein, and W. Warta, *J. Appl. Phys.* **86**, 683 (1999).
- <sup>21</sup>T. C. Kho, S. C. Baker-Finch, and K. R. McIntosh, *J. Appl. Phys.* **109**, 053108 (2011).
- <sup>22</sup>I. Martin, B. Hoex, M. C. M. van de Sanden, R. Alcubilla, and W. M. M. Kessels, in 23rd European Photovoltaic Solar Energy Conference, Valencia, Spain (2008).
- <sup>23</sup>F.-J. Ma, G. G. Samudra, M. Peters, A. G. Aberle, F. Werner, J. Schmidt, and B. Hoex, *J. Appl. Phys.* **112**, 54508 (2012).
- <sup>24</sup>S. Steingrube, P. P. Altermatt, D. S. Steingrube, J. Schmidt, and R. Brendel, *J. Appl. Phys.* **108**, 14506 (2010).
- <sup>25</sup>S. Dauwe, J. Schmidt, A. Metz, and R. Hezel, in *Conference Records of the Twenty-Ninth IEEE Photovoltaic Special Conference* (IEEE, 2002), pp. 162–165.
- <sup>26</sup>K. J. Weber, H. Jin, C. Zhang, N. Nursam, W. E. Jellett, and K. R. McIntosh, in 24th European Photovoltaic Solar Energy Conference, Hamburg, Germany (2009).
- <sup>27</sup>H. Haug, S. Olibet, Ø. Nordseth, and E. S. Marstein, *J. Appl. Phys.* **114**, 174502 (2013).
- <sup>28</sup>H. Haug, Ø. Nordseth, E. V. Monakhov, and E. S. Marstein, *Sol. Energy Mater. Sol. Cells* **106**, 60–65 (2012).
- <sup>29</sup>C. T. Sah, R. N. Noyce, and W. Shockley, *Proc. Inst. Radio Eng.* **45**, 1228–1243 (1957).
- <sup>30</sup>R. Seiwatz and M. Green, *J. Appl. Phys.* **29**, 1034 (1958).
- <sup>31</sup>[www.synopsys.com/silicon/tcad.html](http://www.synopsys.com/silicon/tcad.html), Synopsys Inc - Sentaurus Device TCAD.
- <sup>32</sup>D. A. Clugston and P. A. Basore, “PC1D Version 5: 32-bit solar cell modeling on personal computers,” *Proc. 26th IEEE Photovoltaic Specialists Conference*, Anaheim, pp. 207–210, 1997.
- <sup>33</sup>S. Dauwe, “Low-temperature surface passivation of crystalline silicon and its application to the rear side of solar cells,” Ph.D. thesis (University of Hannover, 2004).
- <sup>34</sup>W. Mönch, *Semiconductor Surfaces and Interfaces*, 3rd ed. (Springer, 2001).
- <sup>35</sup>L. F. Shampine, M. W. Reichelt, and J. Kierzenka, see [http://www.math-works.com/bvp\\_tutorial](http://www.math-works.com/bvp_tutorial) for solving boundary value problems in Matlab (2016).
- <sup>36</sup>E. H. Nicollian and J. R. Brews, *MOS (Metal Oxide Semiconductor)—Physics and Technology* (Wiley, New York, 1982).
- <sup>37</sup>V. Leonov, P. Fiorini, and C. Van Hoof, *IEEE Trans. Dielectr. Electr. Insul.* **13**, 1049–1056 (2006).
- <sup>38</sup>R. S. Bonilla, F. Woodcock, and P. R. Wilshaw, *J. Appl. Phys.* **116**, 54102 (2014).
- <sup>39</sup>Z. Hameiri, F.-J. Ma, and K. R. McIntosh, in *IEEE 40th Photovoltaic Special Conference* (IEEE, 2014), pp. 1842–1847.
- <sup>40</sup>F.-J. Ma, Z. Hameiri, G. S. Samudra, M. Peters, and B. Hoex, in *2014 IEEE 40th Photovoltaic Special Conference* (IEEE, 2014), pp. 3313–3316.
- <sup>41</sup>E. H. Nicollian and A. Goetzberger, *Appl. Phys. Lett.* **7**, 216 (1965).
- <sup>42</sup>D. Vuillaume and J. C. Bourgoin, *J. Appl. Phys.* **58**, 2077 (1985).
- <sup>43</sup>O. Engström, *The MOS System* (Cambridge University Press, 2014).
- <sup>44</sup>J. T. Ryan, A. Matsuda, J. P. Campbell, and K. P. Cheung, *Appl. Phys. Lett.* **106**, 163503 (2015).
- <sup>45</sup>T. J. Tredwell and C. R. Viswanathan, *Solid. State. Electron.* **23**, 1171–1178 (1980).
- <sup>46</sup>A. Ricksand and O. Engström, *J. Appl. Phys.* **70**, 6915 (1991).
- <sup>47</sup>K. R. McIntosh and L. E. Black, *J. Appl. Phys.* **116**, 14503 (2014).
- <sup>48</sup>Y.-Y. Chen, P.-Y. Hsin, C. Leendertz, L. Korte, B. Rech, C.-H. Du, and J.-Y. Gan, *Appl. Phys. Lett.* **104**, 193504 (2014).
- <sup>49</sup>L. M., Terman, *Solid. State. Electron.* **5**, 285–299 (1962).
- <sup>50</sup>C. N. Berglund, *IEEE Trans. Electron Devices* **13**, 701–705 (1966).
- <sup>51</sup>R. Castagne and A. Vapaille, *Surf. Sci.* **28**, 157–193 (1971).
- <sup>52</sup>W. D. Eades and R. M. Swanson, *J. Appl. Phys.* **58**, 4267 (1985).
- <sup>53</sup>W. Fahrner and A. Goetzberger, *Appl. Phys. Lett.* **17**, 16–18 (1970).
- <sup>54</sup>H. Deuling, E. Klausmann, and A. Goetzberger, *Solid. State. Electron.* **15**, 559–571 (1972).
- <sup>55</sup>M. El-Sayed, G. Pananakakis, and G. Kamarinos, *Solid State Electron.* **28**, 345–357 (1985).
- <sup>56</sup>K. R. McIntosh, S. C. Baker-Finch, N. E. Grant, A. F. Thomson, S. Singh, and I. D. Baikie, *J. Electrochem. Soc.* **156**, G190 (2009).
- <sup>57</sup>S. M. S. Sze, N. Kwok, and K. K. Ng, *Physics of Semiconductor Devices*, 3rd ed. (John Wiley and Sons, Inc., Hoboken, New Jersey, 2007).
- <sup>58</sup>P. V. Gray, *Appl. Phys. Lett.* **8**, 31 (1966).
- <sup>59</sup>H. Sakaki, T. Sugano, and K. Hoh, *IEEE Trans. Electron Devices* **17**, 892–896 (1970).
- <sup>60</sup>E. H. Nicollian and A. Goetzberger, *Bell Syst. Tech. J.* **46**, 1055–1133 (1967).
- <sup>61</sup>R. S. Bonilla, K. Collett, L. Rands, G. Martins, R. Lobo, and P. R. Wilshaw, *Solid State Phenom.* **242**, 67–72 (2015).
- <sup>62</sup>H. Amjadi, *Dielectr. Electr. Insul. IEEE Trans.* **6**, 236–241 (1999).
- <sup>63</sup>H. Amjadi, *Dielectr. Electr. Insul. IEEE Trans.* **7**, 222–228 (2000).
- <sup>64</sup>U. Mescheder, B. Müller, S. Baborie, and P. Urbanovic, *J. Microeng. Microeng.* **19**, 94003 (2009).
- <sup>65</sup>KP Technology Ltd - [www.kelvinprobe.com](http://www.kelvinprobe.com).
- <sup>66</sup>I. D. Baikie, S. Mackenzie, P. J. Z. Estrup, and J. A. Meyer, *Rev. Sci. Instrum.* **62**, 1326–1332 (1991).
- <sup>67</sup>R. S. Bonilla, N. Jennison, D. Clayton-Warwick, K. A. Collett, L. Rands, and P. R. Wilshaw, *Energy Procedia* **92**, 326–335 (2016).
- <sup>68</sup>R. A. Sinton, A. Cuevas, and M. Stuckings, in *Conference Records of the Twenty-Fifth IEEE Photovoltaics Special Conference*, 1996, pp. 457–460.
- <sup>69</sup>A. Cuevas and D. Macdonald, *Sol. Energy* **76**, 255–262 (2004).
- <sup>70</sup>A. L. Blum, J. S. Swirhun, R. A. Sinton, F. Yan, S. Herasimenka, T. Roth, K. Lauer, J. Haunschild, B. Lim, K. Bothe, Z. Hameiri, B. Seipel, R. Xiong, M. Dhamrin, and J. D. Murphy, *IEEE J. Photovoltaics* **4**, 525–531 (2014).
- <sup>71</sup>P. P. Altermatt, F. Geelhaar, T. Trupke, X. Dai, A. Neisser, and E. Daub, in *NUSOD'05, Proceedings of the 5th International Conference on Numerical Simulation of Optoelectronic Devices* (IEEE, 2005) pp. 47–48.

- <sup>72</sup>T. Trupke, M. A. Green, P. Würfel, P. P. Altermatt, A. Wang, J. Zhao, and R. Corkish, *J. Appl. Phys.* **94**, 4930 (2003).
- <sup>73</sup>K. L. Luke and L.-J. Cheng, *J. Appl. Phys.* **61**, 2282 (1987).
- <sup>74</sup>See [www.pvlighthouse.com.au](http://www.pvlighthouse.com.au) for diffusion coefficient calculator.
- <sup>75</sup>N. E. Grant, F. E. Rougieux, D. Macdonald, J. Bullock, and Y. Wan, *J. Appl. Phys.* **117**, 55711 (2015).
- <sup>76</sup>N. E. Grant, F. E. Rougieux, and D. Macdonald, *Solid State Phenom.* **242**, 120–125 (2015).
- <sup>77</sup>T. Ohmi, S. Sudoh, and H. Mishima, *IEEE Trans. Semicond. Manuf.* **7**, 440–446 (1994).
- <sup>78</sup>S. W. Glunz, A. B. Sproul, W. Warta, and W. Wettling, *J. Appl. Phys.* **75**, 1611 (1994).
- <sup>79</sup>O. Schultz, M. Hofmann, S. W. Glunz, and G. P. Willeke, in *Conference Recods of the Thirty-First IEEE Photovoltaics Special Conference* (IEEE, 2005), pp. 872–876.
- <sup>80</sup>J. Y. Lee and S. W. W. Glunz, *Sol. Energy Mater. Sol. Cells* **90**, 82–92 (2006).
- <sup>81</sup>R. S. Bonilla, P. G. Hamer, and P. R. Wilshaw, in *EUPVSEC*, Munich, Germany (2016), pp. 707–710.
- <sup>82</sup>H. Mäckel and K. Varner, *Prog. Photovoltaics Res. Appl.* **21**, 850–866 (2013).